Applied Catalysis B: Environmental 84 (2008) 790–796

Contents lists available at ScienceDirect

Applied Catalysis B: Environmental

journal homepage: www.elsevier.com/locate/apcatb

Enhanced carbon monoxide oxidation activity over gold–ceria nanocomposites

Zhi Chen, Qiuming Gao *

State Key Laboratory of High Performance Ceramics and Superfine Microstructures, Shanghai Institute of Ceramics, Chinese Academy of Sciences, 1295 Dingxi Road, Shanghai 200050, PR China

ARTICLE INFO

Article history:
Received 1 April 2008
Received in revised form 13 June 2008
Accepted 13 June 2008
Available online 22 June 2008

Keywords:
Gold–ceria nanocomposites
Enhanced catalytic activity
Low content of Au
CO oxidation

ABSTRACT

The composites with nanosized gold loaded in nanoporous ceria were prepared on a large scale by a facial and environment-benign sol–gel process. These materials were characterized by XRD, ICP, BET, UV–vis absorption, XPS, HRTEM and EDX. The main factors such as size and surface state of the Au and defect in the ceria could be adjusted by acid treatment of the composites in ascorbic acid solution to improve the activity and decrease the content of noble metal Au in the materials. Enhanced catalytic activities were obtained for the CO oxidation reaction over the catalysts due to the small crystal sizes with narrow size distributions of gold nanoparticles, a large amount of defects in the nanoporous ceria support, as well as a high ratio of Au^{3+}/Au^{0} in the nanocomposites.

1. Introduction

Catalysts with high performance and low cost for environmental clean-up are a topic of increasingly world-wide interests from logical design based on the relationship between structure at the molecular level and catalytic property. Gold was traditionally thought as catalytically inert in chemical processes, while highly dispersed Au nanoparticles supported on metal oxides showed exceptionally high activities for several kinds of reactions, including CO oxidation at low temperature. These phenomena are attributed to the quantum size confinement effect [1–3]. As to the CO oxidation over the Au catalyst, the impacting factors influencing the activity depend on the preparation method, surface defect site and changed electronic structure of the small particles, interaction between the metal and support, and so forth [4–6]. The effective supports were usually the oxides of group VIII and 3d transitional metals such as Fe_2O_3, ZrO_2, ZnO, TiO_2, Co_3O_4 and CeO_2 [7–9].

As one kind of the effective support, CeO_2 samples possessed many attractive properties which make them highly promising in applications such as solid-oxide fuel-cell, automotive three-way catalyst, ultraviolet absorber, oxygen sensor, etc. Particularly, the high oxygen storage abilities of CeO_2 samples associated with their rich oxygen vacancies and low redox potentials between the Ce^{3+} and Ce^{4+} have been hence used in the exhaust gas treatments. Nanocrystalline CeO_2 samples are being expected to pose superior physical properties. Some related results have been obtained for them, such as blue-shift in the UV absorption spectra, lattice expansion, Raman-allowed modes shifting and broadening, four orders of magnitude increase in the electronic conductivity and pressure-induced phase transformation, which are partially attributed to the quantum size effect and surface effect [10–12].

The activity of CO oxidation could be enhanced two orders of magnitude when depositing gold nanoparticles on mesoporous CeO_2 nanocrystals comparing with those supported regular ceria sample or prepared by coprecipitation [13]. Although high catalytic activity at low temperature of this composite was observed, the catalytic resistance at high temperature is also very important which is specially emphasized for the waste gas disposal of automobile. However, there were few reports on the fast catalysis of CO oxidation at a high content of CO with high temperature resistance although high catalytic activity at low temperature was observed, favoring elimination of waste gas for automobile and other applications. The fabrication of catalyst in low Au loading with high on-stream activity and high speed of gas flow may be important for the application. Besides, the methods can be industrially applied if the catalyst shows good activity, productivity and durability. Recently, the preparation and characterization of the nanosized CeO_2 samples attracted great interests for their improved properties. Optical and catalytic performances of CeO_2 nanocrystals with the sizes of about 4–5 nm were studied [10]. Nanowires and nanotubes of CeO_2 were formed and their large-scale syntheses were also realized [14–16]. In this paper, we reported the preparation of uniform-sized CeO_2 nanocrystals with porous structures. Using them as supports, the Au–CeO_2 nanocomposite catalysts showed high, durable and

* Corresponding author. Tel.: +86 21 52412513; fax: +86 21 52413122.
E-mail address: qmgao@mail.sic.ac.cn (Q. Gao).

0926-3373/$ – see front matter © 2008 Elsevier B.V. All rights reserved.
doi:10.1016/j.apcatb.2008.06.012

high temperature resistance catalytic activity in the reaction of CO oxidation.

2. Experimental

2.1. Preparation

The nanoporous CeO_2 samples were prepared via a modified precipitant process. In a typical experiment, 0.91 g of $Ce(NO_3)_3{\cdot}6H_2O$ was first added into 10 mL of deionized water. The solution was heated to 100 °C and kept for 5 min with constant stirring under reflux condition. Then, 7.0 mL of $NH_3{\cdot}H_2O$ (5 mol.%) was added with vigorous stirring. And then, the reaction was terminated after 3 min by cooling down the solution to 0 °C. At last, the precipitation powders were recovered by centrifugation, washed with deionized water for three times to remove the additional ions, and dried at 50 °C overnight. The yield was about 90%.

For preparation of the gold-loaded ceria composite, 0.33 g of the as-synthesized ceria samples were put into 20 mL of $HAuCl_4$ solution including 0.1 mmol of Au. Before mixing, the pH value of the solution was adjusted to 7 by using 0.2 M NaOH solution. The mixture was constantly stirred for 2 d at room temperature. The solid powders (denoted as Au–CeO_2-N, where N means neutral) were recovered by centrifugation after washed with deionized water for three times.

Acid treatment was chosen to adjust the composition and structure of the composite. 0.33 g of the as-synthesized ceria samples were put into 20 mL of $HAuCl_4$ solution including 0.1 mmol of Au with pH 7, then the mixture was constantly stirred at room temperature for 2 d, and then the solid powders were separated by centrifugation and washed with deionized water. After that, the obtained solid powders were put into 30 mL of 8.0 mM ascorbic acid solution and stirred constantly for 2 h. The acid-treated powders (denoted as Au–CeO_2-A, where A means acidic) were separated by centrifugation and washed with deionized water for three times.

Both Au–CeO_2-N and Au–CeO_2-A were preserved at room temperature. Large-scale (20 times) preparation of the samples was also carried out by the facial and environment-benign process, where no hazard sources were chosen.

2.2. Characterization

X-ray diffraction (XRD) patterns were obtained on a Rigaku D/max 2200 PC with Cu Kα radiation. Inductively coupled plasma (ICP) analyses were operated on a Vista Axial CCD Simultaneous ICP-AES spectrometer. Nitrogen-sorption isotherms were measured at 77 K on a Micromeritics ASAP-2020M instrument under continuous adsorption conditions. Before measurements, the samples were outgassed at 383 K for 5 h under vacuum. The specific surface areas were calculated by the Brunauer–Emmett–Teller (BET) method. The mesopore and micropore sizes are defined as the positions of the maximum in the pore-size distribution and calculated by the Barrett-Joyner-Halenda (BJH) and Horvath–Kawazoe (HK) methods, respectively, based on the adsorbed branches of the isotherms. Ultraviolet–visible (UV–vis) reflectance spectra of the samples were conducted on a Shimadzu UV-3101 instrument equipped with an integrating sphere using $BaSO_4$ as the reference. X-ray photoelectron spectroscopy (XPS) analyses were carried out on a Microlab 310-F Scanning Auger Microprobe equipped with a 150 W (15 kV by 10 mA) aluminum Kα (1486.6 eV) anode as the X-ray source, using a pass energy of 50 eV with a step size of 0.1 eV. The samples were analyzed in the XPS chamber under an ultrahigh vacuum (10^{-7} Pa base pressure). The samples were dried at 40 °C under vacuum for 8 h before the XPS measurement. The XPS spectra of Ce 3d were calibrated by using C 1s spectrum as the standard. High-resolution transmission electron microscopy (HRTEM) images were taken by using a field emission JEM 2010 electron microscope at 200 kV. Energy dispersive X-ray (EDX) fluorescence spectroscopy was performed on an OXFORD Links ISIS EDX attached to the HRTEM.

2.3. Catalytic reactions

The catalysts were monitored in a fixed-bed quartz tubular reactor with diameter of 12 mm. About 100 mg of the catalysts were placed in the reactor. The reactant gases (2.8% CO, 7.2% O_2 and 90% N_2) went through the reactor with space velocity of 86 mL min^{-1} (ambient temperature and pressure), corresponding to a space velocity of 51 600 mL h^{-1} g_{cat}^{-1}. The concentrations of the outlet CO after stepwise changes in the reaction temperatures were analyzed with an on-line gas chromatograph (SP-6890, molecular sieves 13X column) equipped with a thermal conductivity detector (TCD). Multiple concentrations of the outlet gas were taken and averaged to ensure that the catalytic system had reached steady state. The conversion of CO was calculated using the integrated peak area differences between the CO fed initially and the effluent CO from the reactor with an accuracy of about ±5%.

3. Results and discussion

3.1. XRD analyses

XRD patterns of the as-prepared CeO_2 and the related composites Au–CeO_2-N and Au–CeO_2-A are shown in Fig. 1. The two-theta peaks at 28.68°, 33.10°, 47.44°, 56.44°, 59.02°, 69.40°, 76.71° and 79.00° could be indexed to the (1 1 1), (2 0 0), (2 2 0), (3 1 1), (2 2 2), (4 0 0), (3 3 1) and (4 2 0) planes of fluorite cubic CeO_2 structure (JCPDS# 81-0792), respectively. No change was found after loading Au, indicating that the structures of CeO_2 were well preserved in the composites. The sizes of the CeO_2 particles were about 14.6 nm, calculated based on the Scherrer formula using the (1 1 1) diffraction peaks. The two-theta peaks at 38.30° in correspondence with (1 1 1) plane of fcc Au structure (JCPDS# 89-3697) could be observed for both composite samples Au–CeO_2-N and Au–CeO_2-A, indicating that the well-crystallized gold particles existed in the composites.

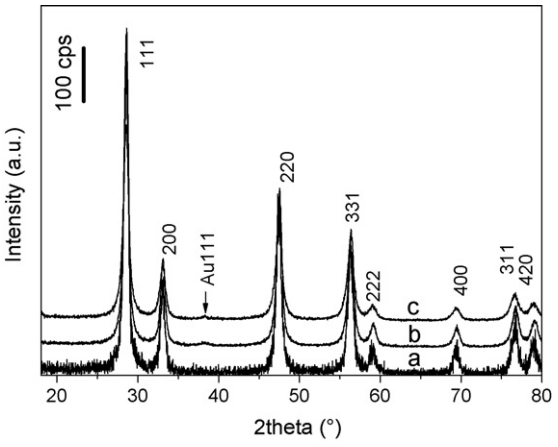

Fig. 1. XRD patterns of the as-synthesized CeO_2 (a) and the nanocomposite samples Au–CeO_2-N (b) and Au–CeO_2-A (c).

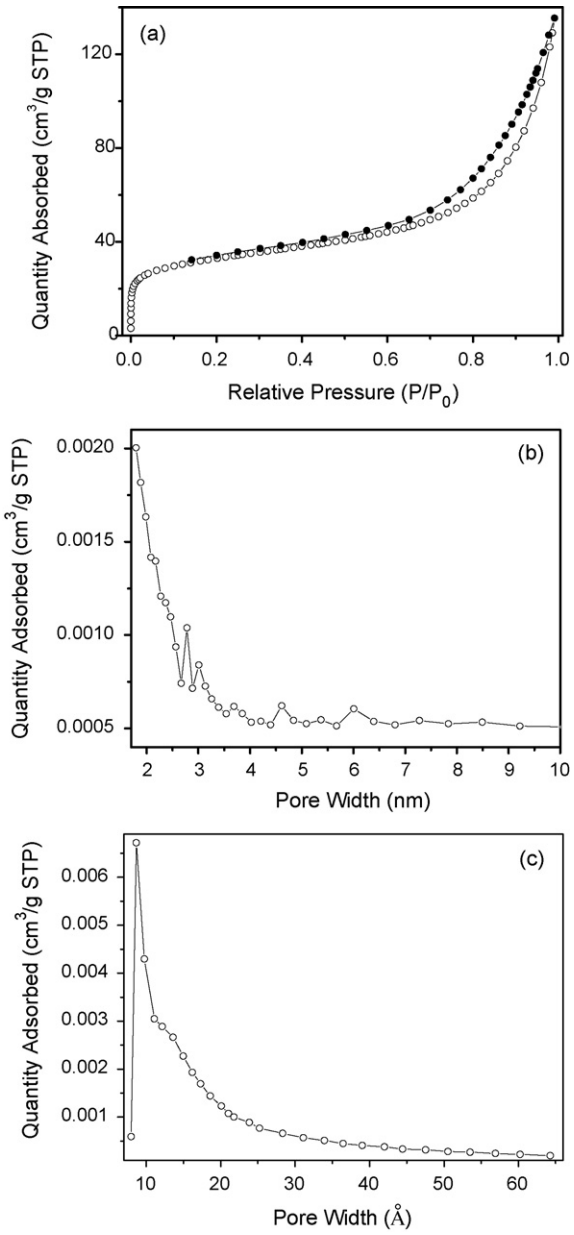

Fig. 2. Nitrogen adsorption (open circle)–desorption (filled circle) isotherms at 77 K of the as-synthesized CeO_2 (a), and its mesopore and micropore width distribution plots derived from BJH (b) and HK (c) methods, respectively.

3.2. Nitrogen adsorption analyses

Nitrogen adsorption–desorption isotherms at 77 K of the as-synthesized CeO_2 are presented in Fig. 2a. A large BET surface areas of 105 m^2/g was got for the as-synthesized CeO_2, which had both mesopores and micropores with the median widths of about 3 and 0.8 nm calculated based on the BJH (Fig. 2b) and HK methods (Fig. 2c), respectively. The surface areas decreased to about 25 m^2/g after loading Au for both samples Au–CeO_2-N and Au–CeO_2-A, which suggests that the Au stayed inside or covered on the widows of the pores of the ceria supports. The loading amounts of Au were about 1.54 and 0.88 wt.% for samples Au–CeO_2-N and Au–CeO_2-A, respectively, based on the ICP and EDX analyses. These results indicate that the acid treatment in ascorbic acid solution could result in a little low content loading of Au in the composite.

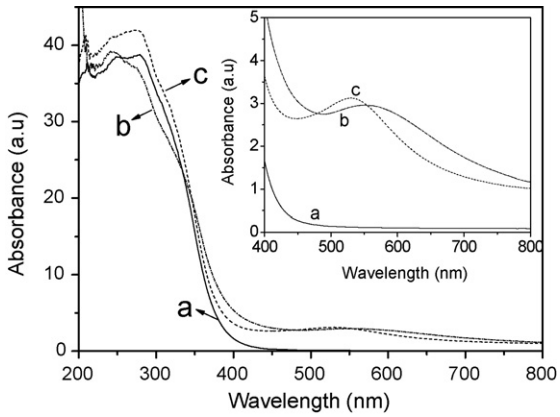

Fig. 3. Diffuse reflectance UV–vis spectra plotted as the Kubelka–Munk function of the as-synthesized CeO_2 (a) as well as the nanocomposite samples Au–CeO_2-N (b) and Au–CeO_2-A (c). The insert is the partially enlargement of the spectra.

3.3. UV–vis absorption spectra analyses

UV–vis absorption spectra of the as-synthesized CeO_2 and the samples Au–CeO_2-N and Au–CeO_2-A are shown in Fig. 3. All of them had absorption bands with the threshold edges at around 380 nm due to the charge-transfer between the O 2p and Ce 4f states in ceria. The blue-shifts of about 10 nm were found, compared to that of the bulk one [17], which are due to the quantum confinement effects of the nanosized CeO_2. The absorption peaks centered at 549 and 530 nm were observed for samples Au–CeO_2-N and Au–CeO_2-A (Fig. 3b and c), respectively, which are due to the surface plasma absorptions of the nanosized Au. For sample Au–CeO_2-A there was a small blue-shift of about 19 nm (inset of Fig. 3), which may be due to the smaller sizes of Au in the composites. The full maximum at the half width (FWHM) of sample Au–CeO_2-A was smaller than that of sample Au–CeO_2-N, indicating that there is a narrower size distribution of the Au particles in sample Au–CeO_2-A. Thus, the acid treatment in ascorbic acid solution could lead to smaller sizes with narrower size distribution of the Au particles in the composites.

3.4. XPS spectra analyses

The Ce 3d, O 1s and Au 4f XPS spectra of the samples Au–CeO_2-N and Au–CeO_2-A are shown in Fig. 4. The peaks of Ce^{3+} and Ce^{4+} ions were identified by non-linear Gaussian peak fittings method after elimination of the backgrounds with the dependences of 98.6% and 99.3% for Ce 3d in samples Au–CeO_2-N and Au–CeO_2-A, respectively. Two peaks at 885, 903 eV and 885, 901 eV could be found in Fig. 4a and b, respectively, which are due to the Ce^{3+} ions in the frameworks of samples Au–CeO_2-N and Au–CeO_2-A. Those peaks at 883, 889, 899, 901, 908, 917 eV and 882, 889, 898, 900, 906, 917 eV are due to the Ce^{4+} ions in the frameworks of samples Au–CeO_2-N and Au–CeO_2-A, respectively. The ratios of the peak intensities of Ce^{3+} over Ce^{4+} ions of sample Au–CeO_2-A are higher than that of sample Au–CeO_2-N, in correspondence with the higher contents of Ce^{3+} ions in sample Au–CeO_2-A.

From Fig. 4c and d one can see that there are three peaks for both samples Au–CeO_2-N and Au–CeO_2-A. The peaks at 530 and 531 eV are attributed to the lattice oxygen and the hydroxide species of CeO_2, respectively. The peaks at 533 eV are related to the presence of Ce^{3+}-related surface defect [8]. The ratio of the peak intensities of 533 eV over 530 eV of sample Au–CeO_2-A is higher than that of sample Au–CeO_2-N, in correspondence with the higher contents of Ce^{3+}-related defects in sample Au–CeO_2-A. So, the acid

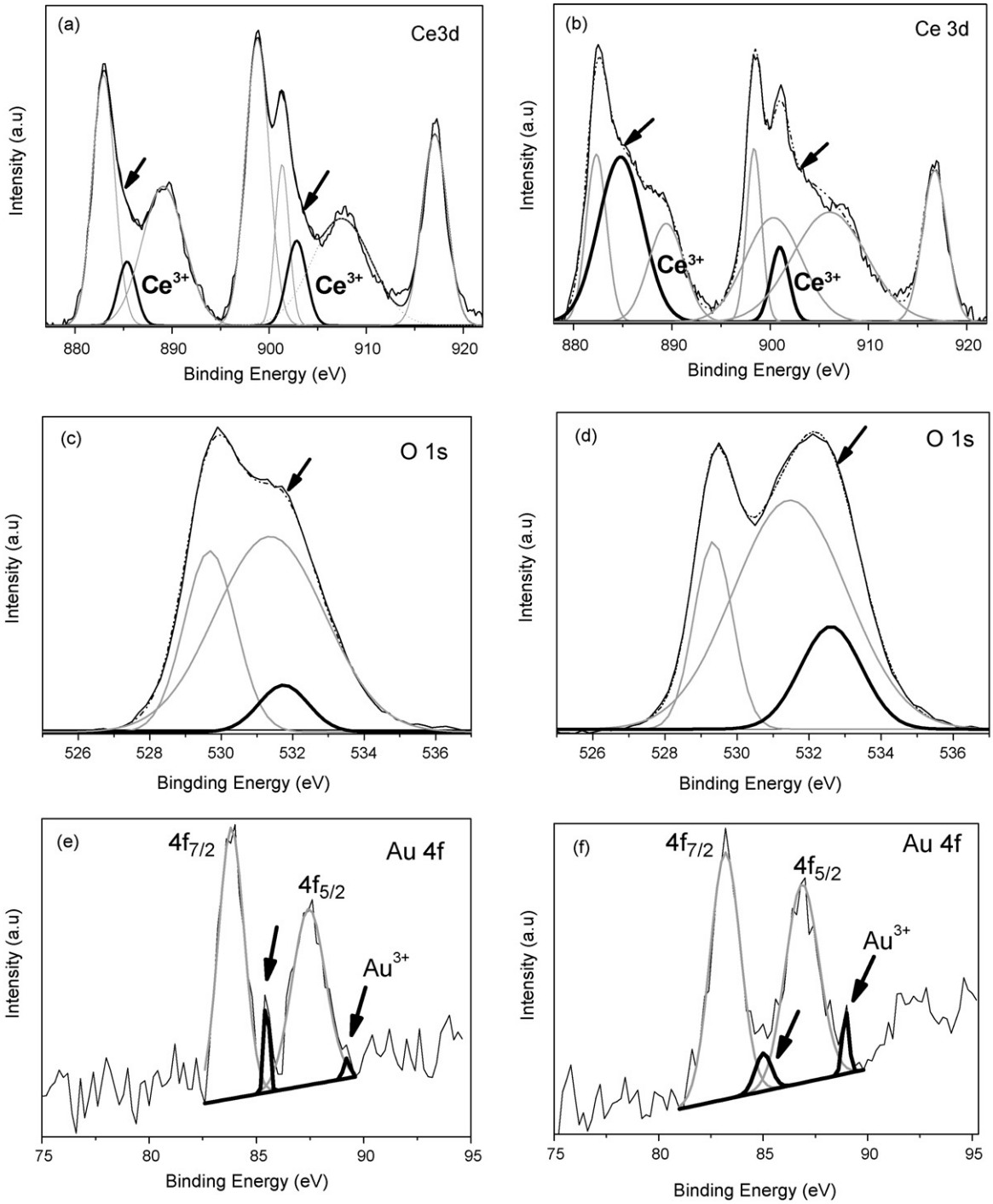

Fig. 4. XPS spectra of Ce 3d and O 1s of the nanocomposite samples Au–CeO_2-N (a and c) and Au–CeO_2-A (b and d) with Gaussian peak fittings. The XPS spectra of Au 4f for Au–CeO_2-N (e) and Au–CeO_2-A (f) are also provided with Gaussian peak fittings.

treatment in ascorbic acid solution may lead to the reduction of some Ce^{4+} ions into Ce^{3+} ions, accordingly, the contents of Ce^{3+} ion-related defects were increased in the ceria support of sample Au–CeO_2-A.

The XPS spectra of Au for Au–CeO_2-N and Au–CeO_2-A are shown in Fig. 4e and f. The main peaks from Gaussian peak fitting of Au $4f_{7/2}$ and $4f_{5/2}$ were found at 83.8/83.2 and 87.4/86.9 eV, respectively, which may be due to the metallic Au in the composites. The tiny two peaks of Au $4f_{7/2}$ and $4f_{5/2}$ at 85.5/85.0 and 89.2/88.9 eV may be attributed to Au^{3+} in the composites [18].

3.5. HRTEM analyses

Both samples Au–CeO_2-N and Au–CeO_2-A had the ceria particles with the sizes of about 14 nm based on the TEM image analyses, which is in correspondence with the analyses based on the XRD calculations. The ceria particles aggregated and some pores were able to be observed. Fig. 5a shows the typical image of the composite sample Au–CeO_2-N. The detailed cross-lattice patterns could be observed on the HRTEM images (Fig. 5b and c). The Au and ceria were highly crystallized in the composite

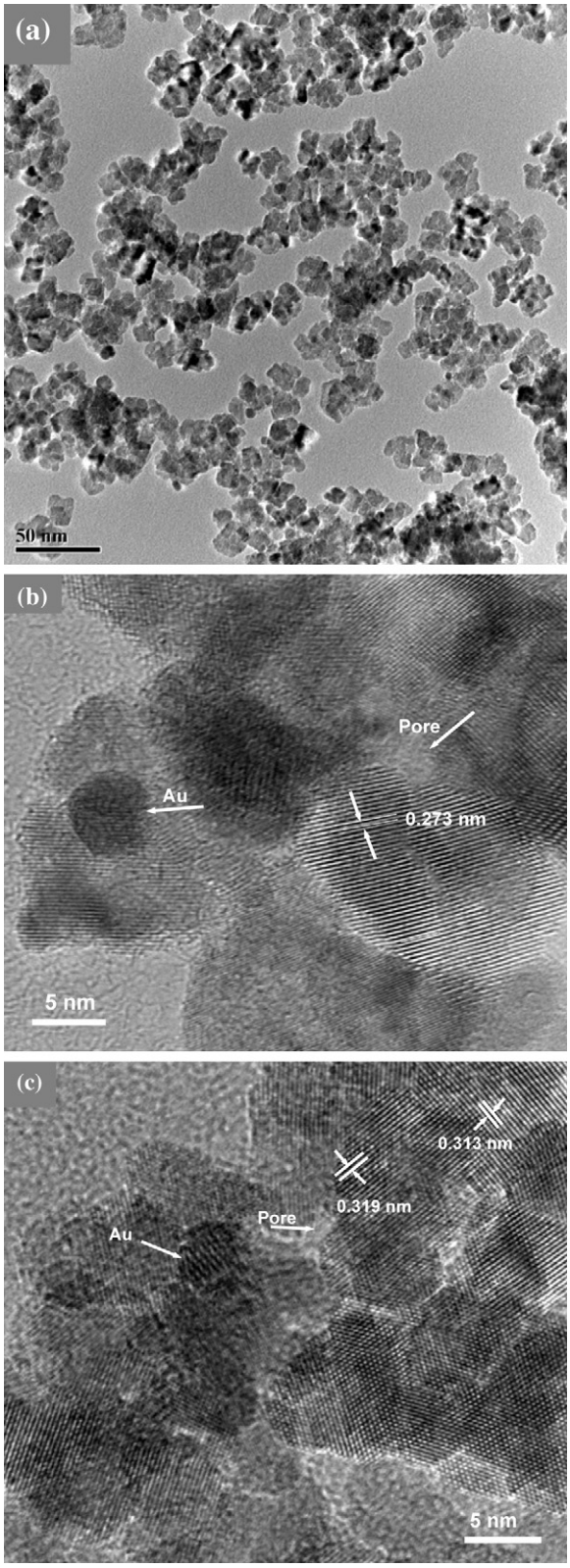

Fig. 5. TEM image of the nanocomposite sample Au–CeO_2-N (a) and HRTEM images of the samples Au–CeO_2-N (b) and Au–CeO_2-A (c).

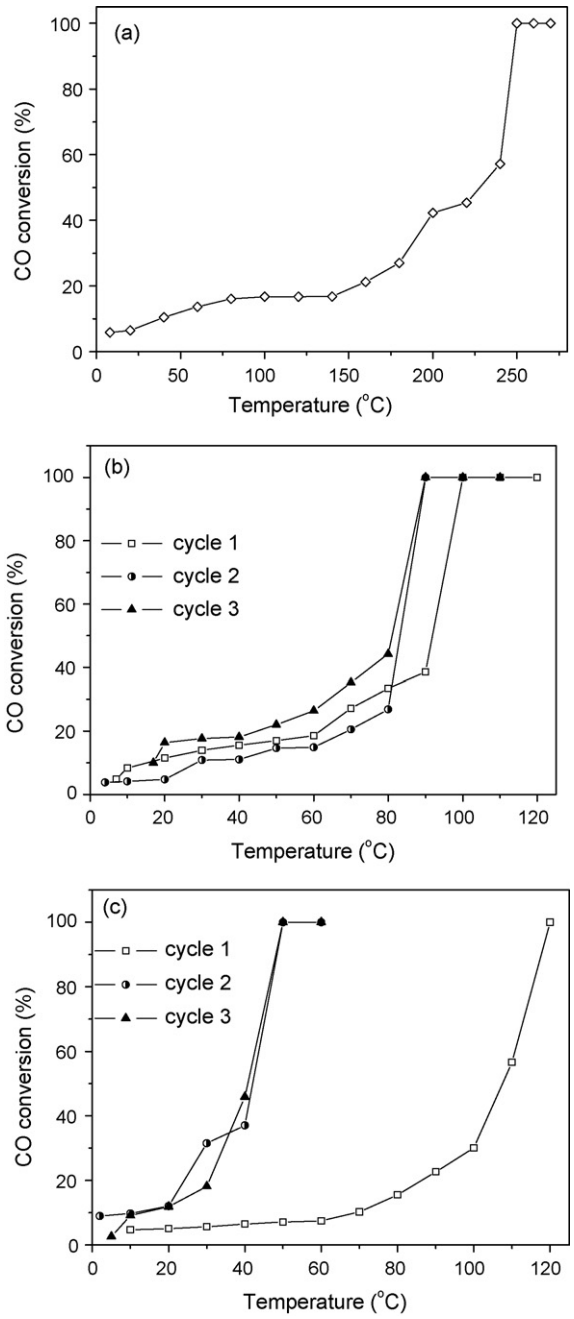

Fig. 6. CO conversion as a function of temperature for different catalytic cycles over the as-synthesized CeO_2 (a) and the nanocomposite samples Au–CeO_2-N (b) and Au–CeO_2-A (c).

samples Au–CeO_2-N and Au–CeO_2-A. Some small pores inside the lattice of ceria could be observed in Fig. 5b and c. A small increase of the lattice parameter of ceria from 0.313 to 0.319 nm was observed in Fig. 5c, but most of the lattice parameter of ceria was 0.313 nm based on the analyses of the distances of (1 1 1) facets, which is due to the existence of Ce^{3+}. These results are in consistent with above spectra analyses that there were more amounts of Ce^{3+} ions in the ceria support of the sample Au–CeO_2-A. The high stability of (2 0 0) planes with the lattice parameter of 0.273 nm were observed for both samples Au–CeO_2-N and Au–CeO_2-A, which possibly be due to the removal of the surface oxygen of ceria [14].

The well-dispersed small spherical Au particles with the sizes of about 5 nm were observed for sample Au–CeO_2-N (Fig. 5b) and the particles with a little smaller sizes were found in sample Au–CeO_2-A (Fig. 5c), which are in correspondence with the above UV–vis spectra analyses. Those Au nanoparticles were highly crystallized and embedded in the CeO_2 supports.

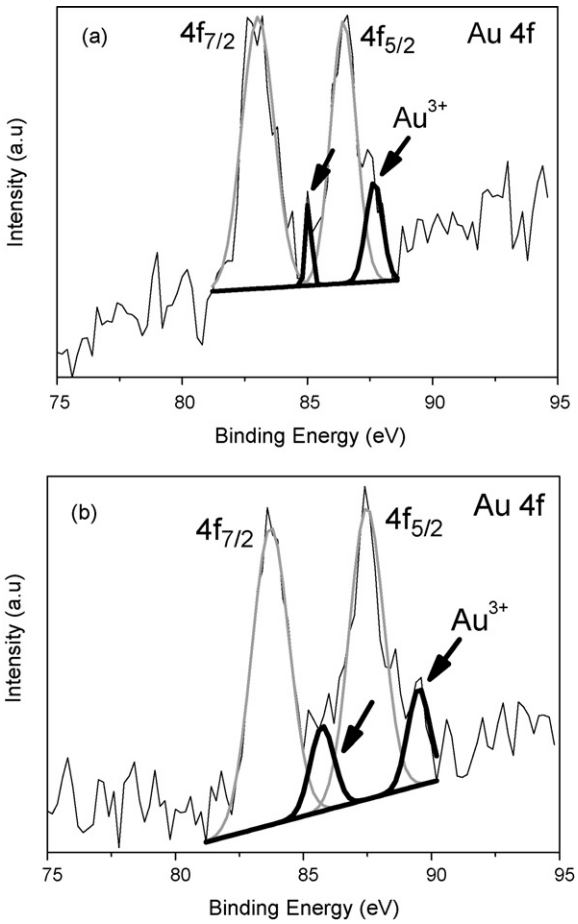

Fig. 7. XPS spectra of Au 4f for Au–CeO_2-N (a) and Au–CeO_2-A (b) with Gaussian peak fittings after the first cycle catalytic reaction.

3.6. CO oxidation reactions

CO oxidation reactions were carried out over the Au–CeO_2-N and Au–CeO_2-A catalysts. For comparation, the reaction was also taken over the as-synthesized CeO_2 support. The complete CO conversion occurred at 240 °C over the as-synthesized CeO_2, as shown in Fig. 6a. This temperature is lower than that of the ceria prepared under alcohothermal conditions, over which the complete CO conversion was found at 280 °C [12]. The higher catalytic activity of our CeO_2 support may be due to its smaller sizes and unique compositions and defect structures [17,19,20].

The percentages of CO conversion with several cycles over the Au–CeO_2-N and Au–CeO_2-A nanocomposite catalysts are shown in Fig. 6b and c. The catalytic activity of CO oxidation was greatly enhanced after loading Au nanoparticles despite the amounts of Au were low (1.54 and 0.88 wt.% for samples Au–CeO_2-N and Au–CeO_2-A, respectively) [1,2]. The catalytic activity occurred at 0 °C and the complete CO conversion was at 120 °C for the first cycle over the sample Au–CeO_2-N. The result of the second run was further enhanced with a lower temperature of complete CO conversion at 90 °C, due to the activation of the composites. The sample as-synthesized showed a stable catalytic activity after the second catalytic run and the complete conversion was preserved at 90 °C for 10 h on-line. Additionally, the complete conversion was at 110 °C when the sample Au–CeO_2-N was heated at 420 °C. In addition, these reactions were performed with a rapidly accelerated CO conversion under high CO concentration (2.8% CO) and gas flow speed (86 mL min^{-1}), so the activity of the as-synthesized is high, compared with the reported results [1,2].

The catalytic activity of CO oxidation over sample Au–CeO_2-A was even higher than that over sample Au–CeO_2-N, despite there was a lower loading amount of Au (0.88 wt.% for sample Au–CeO_2-A). The complete CO conversion was at 120 °C for the first catalytic run (Fig. 6c); but, it sharply decreased to 50 °C for the second catalytic cycle, and then maintained for the third cycle over catalyst Au–CeO_2-A. The same catalytic activity of CO oxidation was observed for the sample Au–CeO_2-A when it was heated at 440 °C. This result shows that the catalyst Au–CeO_2-A is also thermo-stable.

The XPS spectra of Au for Au–CeO_2-N and Au–CeO_2-A after the first cycle catalytic reaction are given in Fig. 7a and b. The peak positions of metallic Au were shifted to 83.0/83.7 and 86.4/87.5 eV and the peak positions of Au^{3+} shifted to 85.1/85.7 and 87.7/89.5 eV from the deconvoluted Au 4f peaks. The peak shift compared with that in Fig. 4e and f may come from the interaction of Au with ceria support. The intensities of peaks assigned to Au^{3+} increased after the first catalytic cycle for both samples. The intensity (peak area) ratio of Au^0/Au^{3+} corresponding peaks decreased from 16.18/14.68 to 6.31/4.76 for Au–CeO_2-N and Au–CeO_2-A, respectively, after the first catalytic cycle. The higher activity of Au–CeO_2-N and Au–CeO_2-A after the first cycle catalytic reaction may be partly due to the increased ratio of Au^{3+}/Au^0, where Au^{3+} is related to the formation of $Au^{\sigma+}$–Au^0 [21].

Thus, the higher catalytic activity of sample Au–CeO_2-A may be resulted from the much stronger interaction between the CeO_2 and Au than that of sample Au–CeO_2-N, due to the smaller crystal sizes with narrower size distribution of Au and more defects in the host for the Au–CeO_2-N. Besides, the activity of Au–CeO_2-N and Au–CeO_2-A is closely related to the ratio of Au^{3+}/Au^0, and the higher ratio of Au^{3+}/Au^0 in sample Au–CeO_2-A after the first cycle catalytic reaction may be contributed to its higher catalytic activity.

4. Conclusions

The Au–CeO_2 nanocomposite catalysts have been successfully prepared on a large scale by a sol–gel process. The preparation method is facile and low cost without using any hazard sources. Even though the catalysts have low amounts of Au (1.54–0.88 wt.%), enhanced catalytic activities have been observed for the CO oxidation reaction due to the small crystal sizes with narrow size distribution of the Au nanoparticles as well as more defects in the CeO_2 support of the composites. Acid treatment in ascorbic acid solution may decrease the sizes and improve the homogeneity of the Au particles and improve the Ce^{3+} ion-related defect contents in the ceria, resulting in the higher activity of the composite and lower content of noble metal Au. The acid treatment may also lead to a higher ratio of Au^{3+}/Au^0 in the sample after the first cycle catalytic reaction, which is helpful for its higher catalytic activity. The catalysts are thermo-stable and their high activities have been preserved very well after the treatment at the temperature no more than 400 °C. These low-cost catalysts may be favorable for the elimination of CO from the exhaust gas during both engine's start-up and durative processes.

Acknowledgement

This work was financially supported by Chinese National Science Foundation (No. U0734002), "Project of One Hundred Outstanding Talents" of Chinese Academy of Sciences and Shanghai Nanotechnology Promotion Center (No. 0652nm025).

References

[1] D. Widmann, R. Leppelt, R.J. Behm, J. Catal. 251 (2007) 437.
[2] C.T. Chang, B.J. Liaw, C.T. Huang, Y.Z. Chen, Appl. Catal. A: Gen. 332 (2007) 216.

[3] D. Astruc, F. Lu, J.R. Aranzaes, Angew. Chem. Int. Ed. 44 (2005) 7852.
[4] W.S. Epling, G.B. Hoflund, J.F. Weaver, S. Tsubota, M. Haruta, J. Phys. Chem. 100 (1996) 9929.
[5] L. Yan, X. Zhang, T. Ren, H. Zhang, X. Wang, J. Suo, Chem. Commun. 8 (2002) 860.
[6] F. Moreau, G.C. Bond, A.O. Taylor, Chem. Commun. 14 (2004) 1642.
[7] D.C. Meier, D.W. Goodman, J. Am. Chem. Soc. 126 (2004) 1892.
[8] A.M. Venezia, G. Pantaleo, A. Longo, G.D. Carlo, M.P. Casaletto, F.L. Liotta, G. Deganello, J. Phys. Chem. B 109 (2005) 2821.
[9] L. Wen, J. Fu, P. Gu, B. Yao, Z. Lin, J. Zhou, Appl. Catal. B: Environ. 79 (2008) 402.
[10] X.D. Zhou, W. Huebner, H.U. Anderson, Appl. Phys. Lett. 80 (2002) 3814.
[11] J. Zhu, Q. Gao, Z. Chen, Appl. Catal. B: Environ. 81 (2008) 236.
[12] Y. Zhang, R. Si, C. Liao, C. Yan, C. Xiao, Y. Kou, J. Phys. Chem. B 107 (2003) 10159.
[13] S. Carrettin, P. Concepcion, A. Corma, López J.M. Nieto, V.F. Puntes, Angew. Chem. Int. Ed. 43 (2004) 2538.
[14] H. Chen, H. Chang, Solid State Commun. 133 (2005) 593.
[15] W. Han, L. Wu, Y. Zhu, J. Am. Chem. Soc. 127 (2005) 12814.
[16] T. Yu, J. Joo, Y.I. Park, T. Hyeon, Angew. Chem. Int. Ed. 44 (2005) 7411.
[17] G. Glaspell, L. Fuoco, M.S. El-Shall, J. Phys. Chem. B 109 (2005) 17350.
[18] B.V. Crist, Handbooks of Monochromatic XPS Spectra, XPS International, LLC, 1999.
[19] K. Zhou, X. Wang, X. Sun, Q. Peng, Y. Li, J. Catal. 229 (2005) 206.
[20] Y. Wang, A. Zhu, Y. Zhang, C.T. Au, X. Yang, C. Shi, Appl. Catal. B: Environ. 81 (2008) 141.
[21] Y. Shen, X. Yang, Y. Wang, Y. Zhang, H. Zhu, L. Gao, M. Jia, Appl. Catal. B: Environ. 79 (2008) 142.